Acta Oceanol. Sin., 2020, Vol. 39, No. 7, P. 69–78
https://doi.org/10.1007/s13131-020-1573-5
http://www.hyxb.org.cn
E-mail: hyxbe@263.net

The oceanic responses to Typhoon Rananim on the East China Sea

Dan Xu[1], Zhiyuan Li[2], Zhanhong Wan[3]*, Zongfu Ren[3], Zhongshui Zou[3]*, Xiuyang Lv[3], Shizhu Luo[3]

[1] College of Civil Engineering and Architecture, Zhejiang University, Hangzhou 310058, China

[2] Collegeof Hydraulic and Environmental Engineering, Zhejiang University of Water Resources and Electric Power, Hangzhou 310018, China

[3] Ocean College, Zhejiang University, Zhoushan 316021, China

Received 31 March 2019; accepted 27 September 2019

Abstract

Many typhoons pass through the East China Sea (ECS) and the oceanic responses to typhoons on the ECS shelf are very energetic. However, these responses are not well studied because of the complicated background oceanic environment. The sea surface temperature (SST) response to a severe Typhoon Rananim in August 2004 on the ECS shelf was observed by the merged cloud-penetrating microwave and infrared SST data. The observed SST response shows an extensive SST cooling with a maximum cooling of 3°C on the ECS shelf and the SST cooling lags the typhoon by about one day. A numerical model is designed to simulate the oceanic responses to Rananim. The numerical model reasonably simulates the observed SST response and thereby provides a more comprehensive investigation on the oceanic temperature and current responses. The simulation shows that Rananim deepens the ocean mix layer by more than 10 m on the ECS shelf and causes a cooling in the whole mixed layer. Both upwelling and entrainment are responsible for the cooling. Rananim significantly deforms the background Taiwan Warm Current on the ECS shelf and generates strong Ekman current at the surface. After the typhoon disappears, the surface current rotates clockwise and vertically, the current is featured by near inertial oscillation with upward propagating phase.

Key words: typhoon, sea surface temperature, numerical model, mix layer, near inertial oscillation

Citation: Xu Dan, Li Zhiyuan, Wan Zhanhong, Ren Zongfu, Zou Zhongshui, Lv Xiuyang, Luo Shizhu. 2020. The oceanic responses to Typhoon Rananim on the East China Sea. Acta Oceanologica Sinica, 39(7): 69–78, doi: 10.1007/s13131-020-1573-5

1 Introduction

Typhoons are very transient and violent atmospheric events in the tropical and subtropical oceans and are widely studied. When a typhoon passes, the strong wind stress generates intensive thermal and physical oceanic responses (Price, 1981; Brink, 1989; Shay, 2010). A very prominent thermal response is the sea surface temperature (SST) cooling (Price, 1981; Wentz et al., 2000). The maximum SST drop caused by a typhoon is about 10.8°C (Chiang et al., 2011). Usually, the SST response is asymmetric. In the northern hemisphere, the SST cooling is much stronger to the right side of the typhoon track (Wright, 1969; Price, 1981). In addition to the SST cooling, a typhoon also deepens the mix layer (ML) and causes the whole ML cooling. The strong vertical mixing and Ekman pumping are responsible for the ML cooling process (Price, 1981; Emanuel, 1999; Jacob et al., 2000). In addition to the thermal response, one prominent physical oceanic response is the energetic near inertial oscillations (NIOs) in the ML which are generated by a fast moving typhoon (Brook, 1983; Price, 1983; Shay and Elsberry, 1987). The NIOs are characterized by strong horizontal near inertial currents (NICs) with upward propagating phase. The upward propagation indicates that typhoon transfers the powerful mechanical energy downward to deeper ocean.

The East China Sea (ECS) is a shelf sea in the northwestern Pacific Ocean. The ECS features a very wide continental shelf with shallow water of less than 200 m. Every year, there are many typhoons forming in the northwestern Pacific Ocean, traversing the ECS shelf and landing the mainland of China. When a typhoon approaches to coastal region, it generates storm surges and causes a sea level rise along the coast which brings great loss to people's lives and properties in coastal cities. Therefore, the studies of shelf seas responses to typhoon are of great social value. The oceanic responses to typhoons on the shallow shelf are more energetic than those in the open ocean (Yang et al., 2015). However, the oceanic responses to typhoons on the ECS shelf are not well studied yet. This is possibly due to two factors: one is the complex background current systems in the ECS, e.g., the strong western boundary current—Kuroshio Current (KC) and Taiwan Warm Current (TWC). The other factor is the inefficiency of satellite SST, which suffers greatly from the cloud on the ECS shelf.

In August 2004, Typhoon Rananim passed over the ECS. Rananim is a severe typhoon formed in the tropical Pacific Ocean on August 8, 2004 with a maximum wind speed of about 58 m/s. It moves northwestward quickly and reached to the east of Taiwan on August 9 (Fig. 1b), then enters the southern ECS

Foundation item: The National Key Research and Development Program of China under contract Nos 2016YFC0402303 and 2017YFC1403300; the National Natural Science Foundation of China under contract Nos 11572283, 11602179 and 41806028; the Public Science and Technology Research Funds Projects of Ocean under contract No. 20110518-5.
*Corresponding author, E-mail: wanzhanhong@zju.edu.cn; zouzhongshui@126com

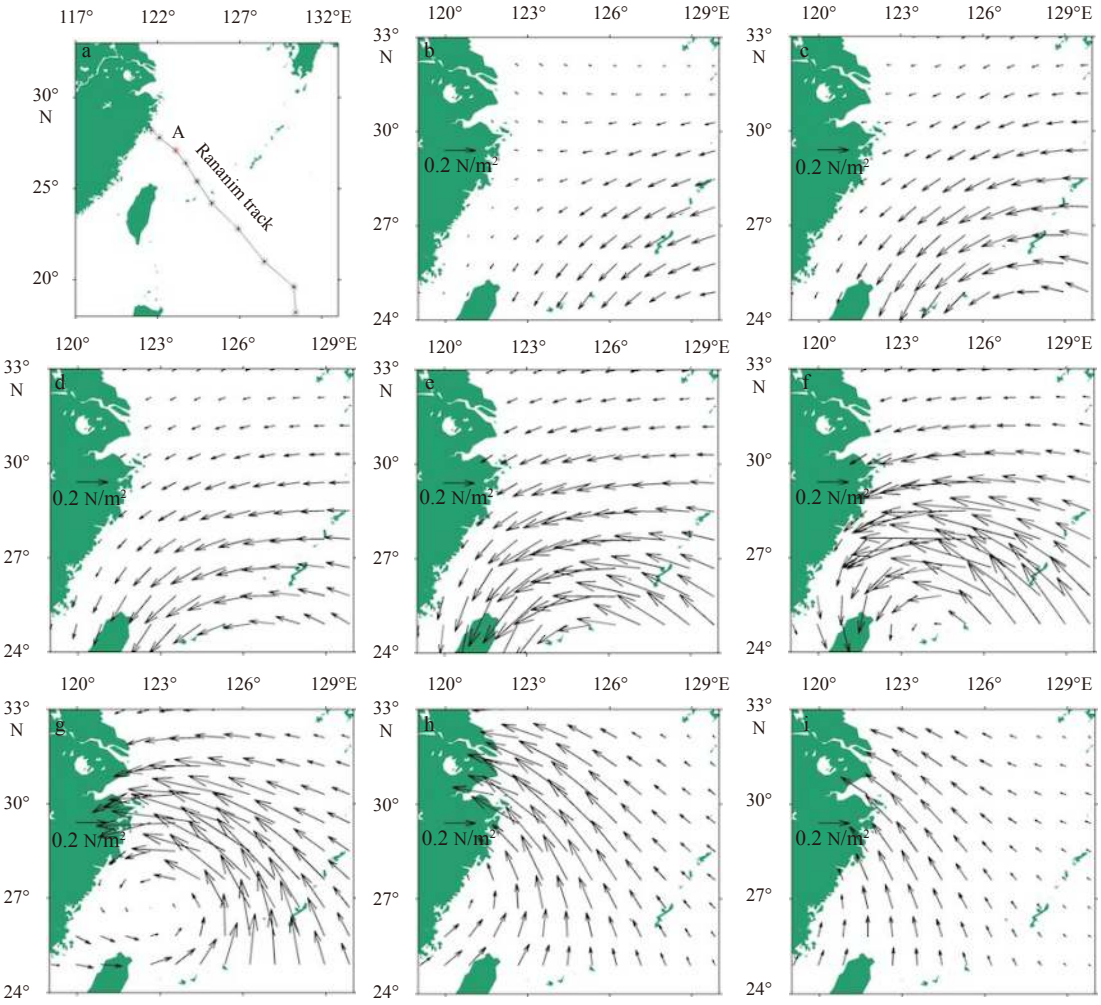

Fig. 1. The wind filed during the Typhoon Rananim. a. The track of Rananim in 2004 summer, and b–i. the spatial and temporal evolution of wind stress from 6-hourly NCEP-NCAR when Rananim passes over the ECS. Each snapshot has an interval of 12 h. A representative grid point A (27.3°N, 123°E) along the Rananim track. The wind speed data used to study Rananim is obtained from the 6-hourly NCEP-NCAR reanalysis data (Kalnay et al., 1996).

(Figs 1c–g). It lands in the Zhejiang Province of China on August 12 with a very strong wind speed of 45 m/s. The track and evolution of Rananim is shown in Fig. 1. The SST response to Rananim on the ECS shelf can be observed from a merged cloud-penetrating microwave and infrared (MWIR) OI SST data (Gentemann et al., 2010). To reveal the oceanic responses to Rananim more completely, a numerical model is also performed. This paper is organized as follows: the passage of Rananim and observed SST response are shown in Section 2. The model configuration is provided in Section 3. Section 4 shows the simulated oceanic responses. In Section 5, the conclusions are presented.

2 Satellite SST response to Rananim

Figure 2 shows the satellite SST serial images from the merged cloud-penetrating MWIR OI SST data. The data has a spatial resolution of 9 km and temporal sample of 1 year. Therefore, this SST data is free of the influence of cloud on a continental shelf, and can provide a direct view of the evolution of SST response to Rananim on the ECS shelf. Before the passage of Rananim on 9 August, the SST distribution in the ECS is shown in Fig. 2a. The SST is high in the offshore region and low in the coastal area. In the following snapshots, Rananim passes over the ECS and causes a wide SST cooling on the shelf. We use the SST anomaly (SSTA) to better characterizing the SST cooling after the passage of Rananim.

The SSTA is defined by the SST after typhoon passage subtracts the SST value before typhoon passage, namely the value on August 9. For example, the SSTA shown in Fig. 2b is the value on August 10 subtracts the value on August 9. Rananim reached to the southern ECS on August 10. However, SST cooling cannot be widely found in the ECS (Fig. 2b). There is a roughly one day phase lag between SST response and the typhoon passage. Evident SST cooling (SST drops 1°C) in the southern ECS is noticed on 11 August (Fig. 2c). In the following two days (August 12, 13), the SST cooling continues to strengthen. The most significant SST cooling (SST drops as much as 3°C) occurs on 13 August (Fig 2e, one day after the snapshot of Fig. 1g). In the last snapshot (Fig. 2f), although Rananim has landed, SST cooling is still noted although its strength is weakening.

3 Numerical simulation

Numerical models are widely used in the study of coastal region and typhoon. In this study, a numerical model (MITgcm) (Marshall et al., 1997) with real-case topography and driving

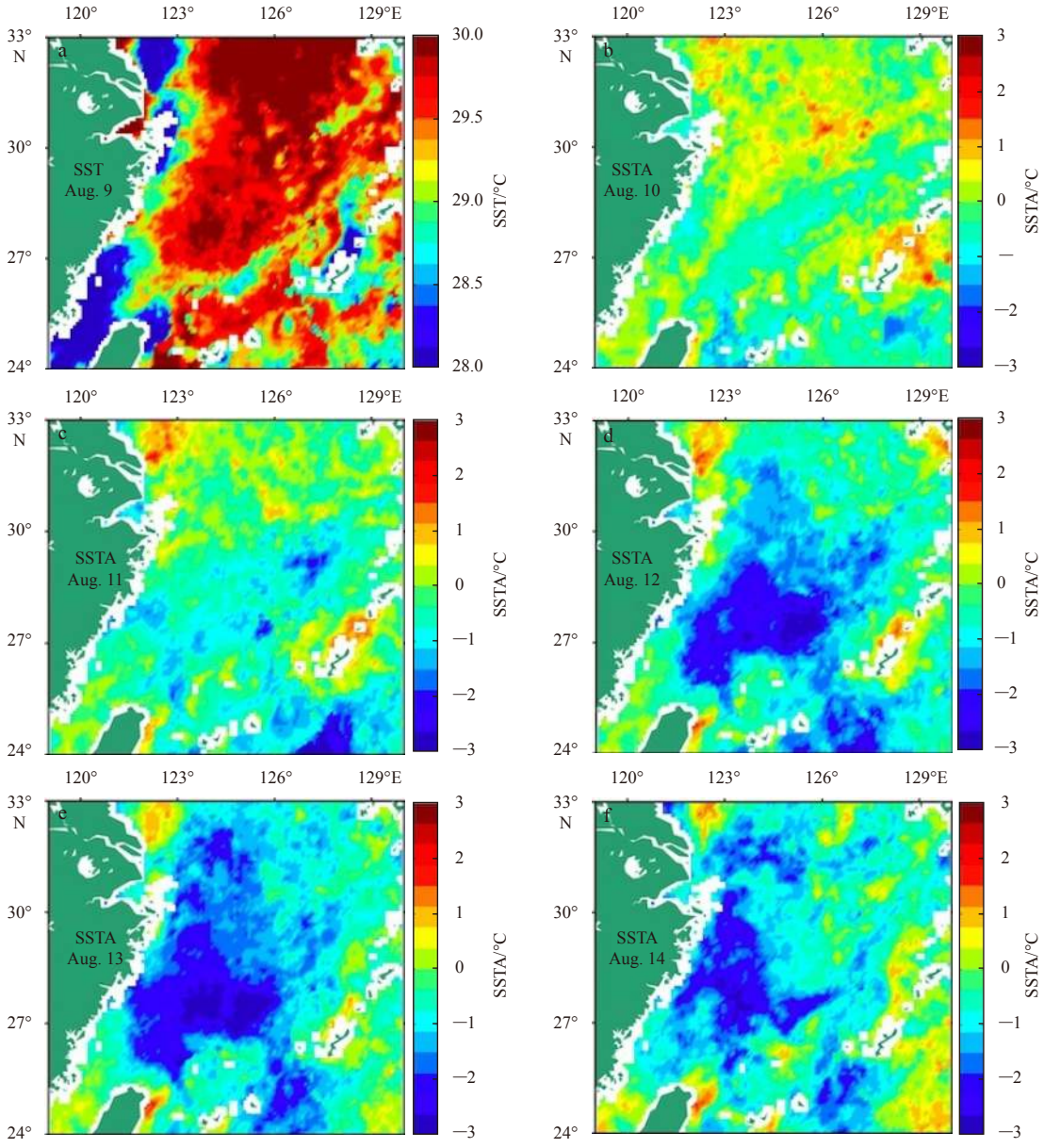

Fig. 2. The variation of SST with time during Typhoon Rananim. a. The satellite observed SST on August 9, 2004, before Rananim; and b–f. SSTA from August 10 to 14, during and afterthe passage of Rananim.

forces is designed to simulate the oceanic responses to Rananim in the ECS. The MITgcm has been successfully applied to the ECS to study oceanic response to strong surface wind (Li et al., 2019; Li and Huang, 2019). The simulated area is from 24°to 43°N and from 117.25° to 131.00°E and (Fig. 3), which covers not only the ECS but also the Bohai Sea and the Yellow Sea. This model domain has only two open boundaries, namely a southern open boundary and an eastern open boundary. The model has a uniform spatial resolution of (1/20°) and 40 vertical levels. The bottom topographic data is from the ETOPO2 and the maximum and minimum depths are set to 3 000 and 5 m, respectively. The monthly initial temperature and salinity data for January are from the World Ocean Atlas 2013 (https://www.nodc.noaa.gov/General/survey/85d79e16-52f4-4a36-b1ad-4c4c6fce2d24/20110208/). The model is driven by the surface forcing, such as the wind stress and net heat and water fluxes provided by the NCEP-NCAR reanalysis data (Kalnay et al., 1996) and by the open boundary conditions, including the temperature, salinity and velocity from the Hybrid Coordinate Ocean Model (HYCOM) outputs (Bleck, 2002).The model is driven by the surface forces and open boundary conditions of 2004 for 10 years (annual-cycle) to reach a steady state. The monthly salinity and temperature for August of the tenth year model outputs are abstracted as the initial condition for the real-case simulation of typhoon. The typhoon simulation is driven by the 6 hourly surface forcing data from the NCEP-NCAR reanalysis data and daily open boundary conditions from HYCOM. The real-case run is integrated from 1 August 2004 to 31 August 2004 for a duration run of 31 days with a time step of 100 s. Because the oceanic responses to typhoon are short term processes (about one week), therefore, the 3-hourly wind stress, simulated temperature and current from 9 August 2004 to 15 August 2004 are used for analysis.

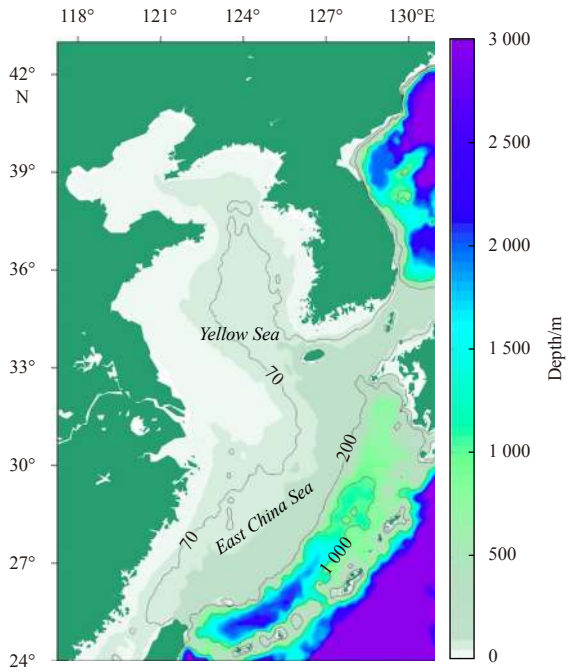

Fig. 3. Model domain and bottom topography with contours of 70 200 and 1 000 m isobaths.

4 Simulation results

4.1 *Oceanic temperature responses*

The SST response to Rananim in the ECS from 9 to 14 August in the real-case simulation is shown in Fig. 4. Similar with the observed SST response, the simulated SST anomaly (SSTA) is used to better characterize the simulated SST cooling after the Rananim passage. The comparison between observed (Fig. 2) and simulated (Fig. 4) SST responses shows reasonably good agreement. Before Rananim passes the ECS, both the spatial pattern and magnitude of the simulated SST are in good agreement with the observed one. Although the simulated SST cooling is slightly weaker than the observed SST cooling, the simulated SST cooling can reasonably reflect the temporal evolution of the observed one. The simulation shows that significant SST cooling in the ECS begins August (similar with the observed one). This reasonably good agreement indicates that the numerical model well reproduces the oceanic responses to Rananim in the ECS.

Another prominent feature of the SST response to typhoon is the asymmetry. Namely, in the northern semisphere, the SST cooling is much stronger on the right side of the typhoon track (Price, 1981). To characterize the right bias of the SST cooling, the temporal evolution of the SST cooling during Rananim passes the ECS is shown in Fig. 5. Because the SST cooling lags Rananim by one day, the wind stress shown in Fig. 5 leads the overlapped simulated SSTA by one day. For example, the wind stress in Fig.5a is on 11 August, and the simulated SSTA is on 12 August. Figure 5 shows the snapshots of the wind stress from 11 to 12 August when Rananim is the strongest. As shown in Fig. 5, the Rananim track is northwestward. Therefore, SST cooling is much stronger in the northern ECS and much weaker in the southern ECS, characterizing a prominent right bias. The right bias of SST cooling is because the wind stress is much stronger at the right side of Rananim track.

A meridional section (123°E) and a latitudinal section (27°N) were selected to see the right-bias vertically (Fig. 6a). The inter-

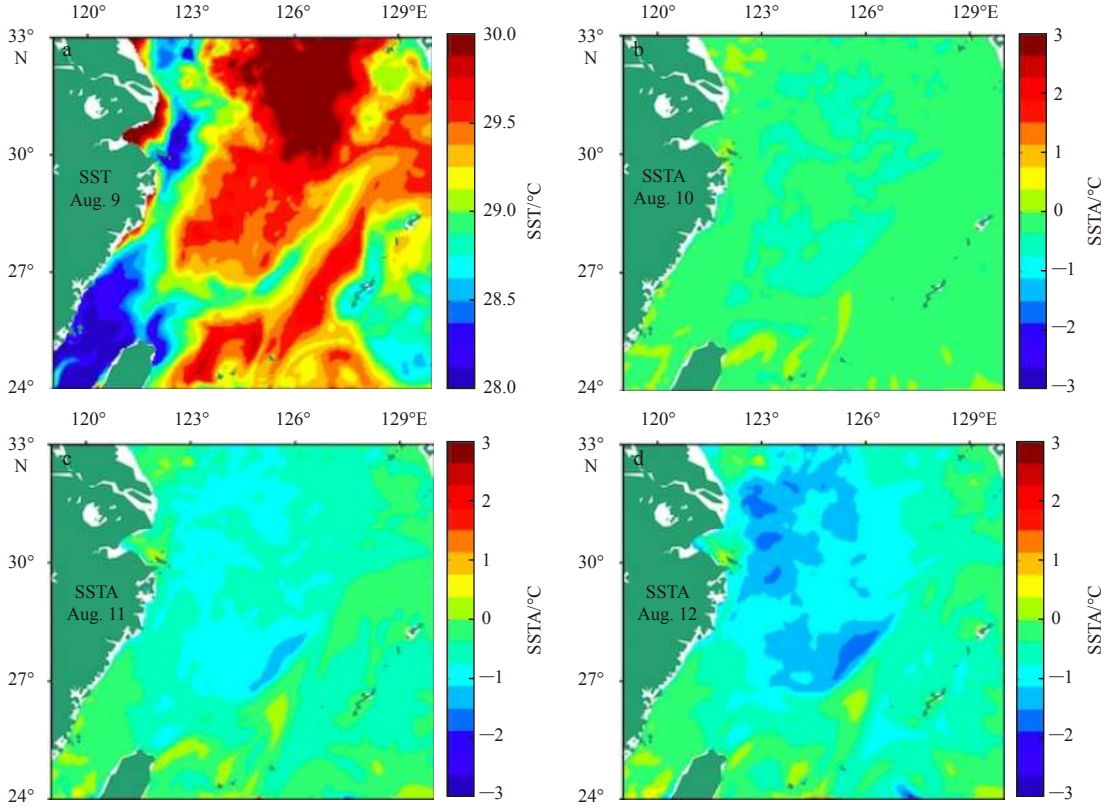

Fig. 4.

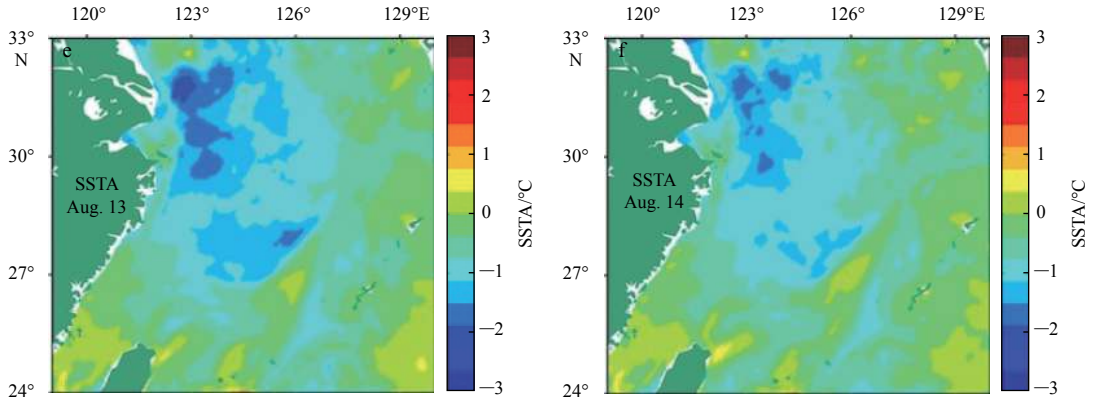

Fig. 4. The model simulated SST and SSTA. a. SST before Rananim(August 9, 2004); and b–f. SSTA after Rananim (August 10–14).

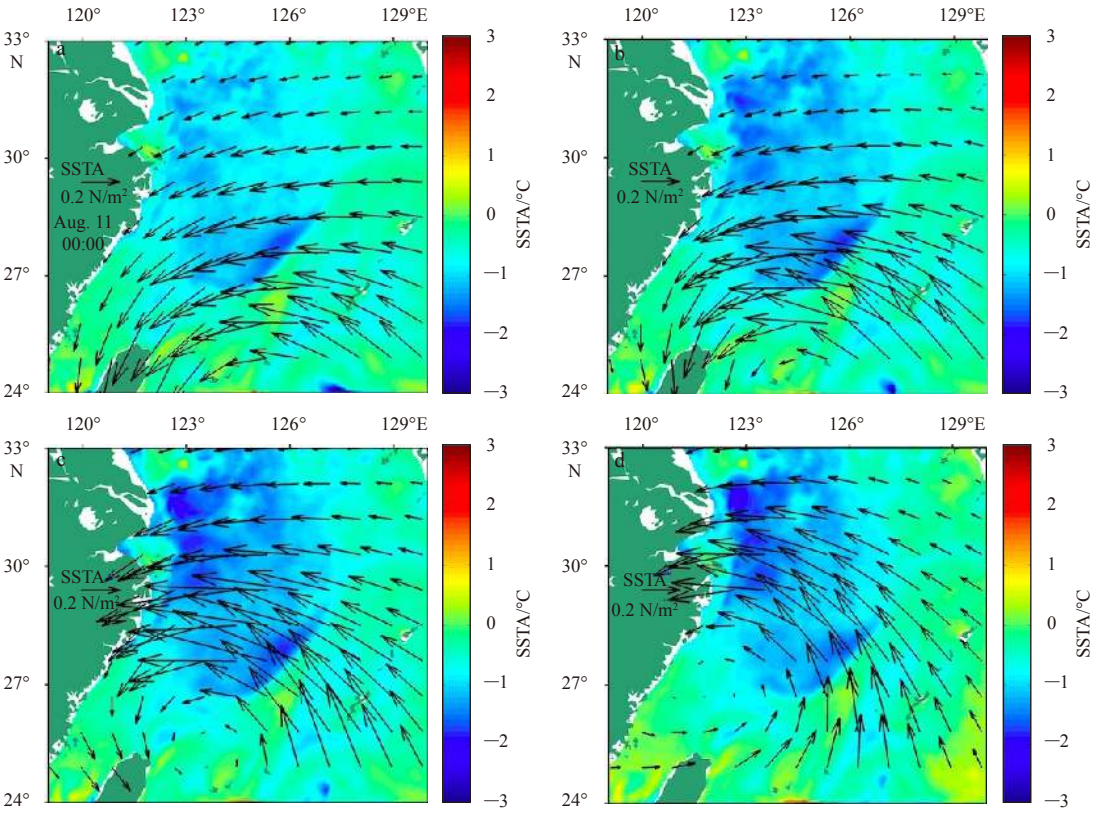

Fig. 5. Snapshots of the wind stress during the Rananim passage overlapped with the simulated SSTA in the ECS. Note that in each snapshot, the SSTA lags 1 day by the wind stress.

section is the center of the typhoon. Thus, the meridional section can test whether the influence of the typhoon on the sea surface temperature in the north direction is larger, and the latitudinal section can test whether the influence of the typhoon on the sea surface temperature in the east direction is larger.

Figure 6b shows the variation of SSTA over time in the 27°N section of the East China Sea. The larger absolute value of SSTA is mainly distributed far from the horizontal axis of the coordinate, that is the east side of the typhoon center, and the smaller absolute value of SSTA is mainly distributed near the abscissa, the west side of the typhoon center. Figure 6c shows the variation of SSTA over time in the 123°E section of the East China Sea. The larger absolute value of SSTA is mainly distributed close to the north side of typhoon; and the smaller SSTA is mainly distributed close to the south. The right-bias of Typhoon Rananim's effect on the surface temperature of the East China Sea can always be detected.

In addition to causing SST cooling, typhoon also affects the ML. First, typhoon leading to a deepening of the ML depth. Second, typhoon causes significant ML cooling because of the vertical mixing, which is always called the vertical entrainment (Price, 1981). Figure 7a shows the temporal evolution of water temperature throughout the whole water column at a representative location. It shows an evident deepening of the ML after the Rananim passage. Moreover, temperature decreasing in the ML is also noticeable. To quantitatively describe these two features,

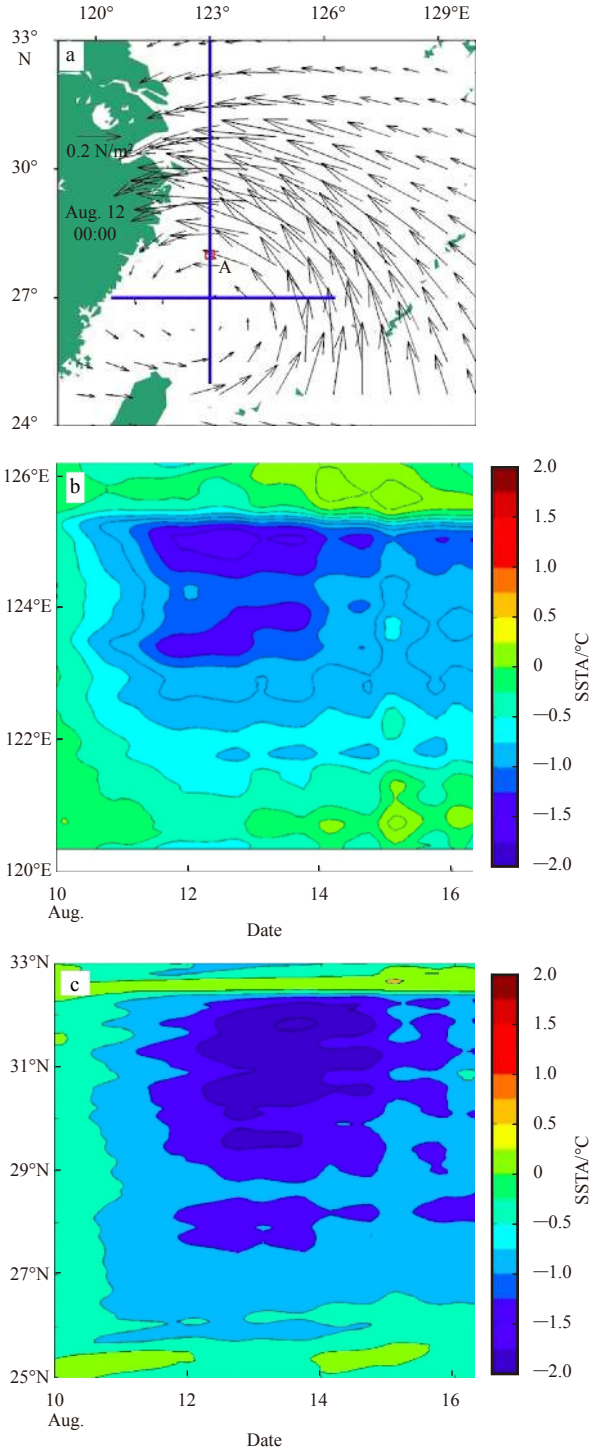

Fig. 6. Wind stress distribution and variation of sea surface temperature anomaly. a. Wind stress distribution at 0 o'clock on August 12 and two representative sections selected at the time in the East China Sea. The box A in the figure is a grid point selected on the right side of the typhoon path. b. Variation of sea surface temperature anomaly (SSTA) over time in the 27°N section of the East China Sea. c. Variation of sea surface temperature anomaly (SSTA) over time in the 123°E section of the East China Sea.

the ML depth and temperature at bottom of the ML are calculated. The ML depth is calculated according the definition, i.e., the depth at which the temperature is 0.5°C lower than the SST.

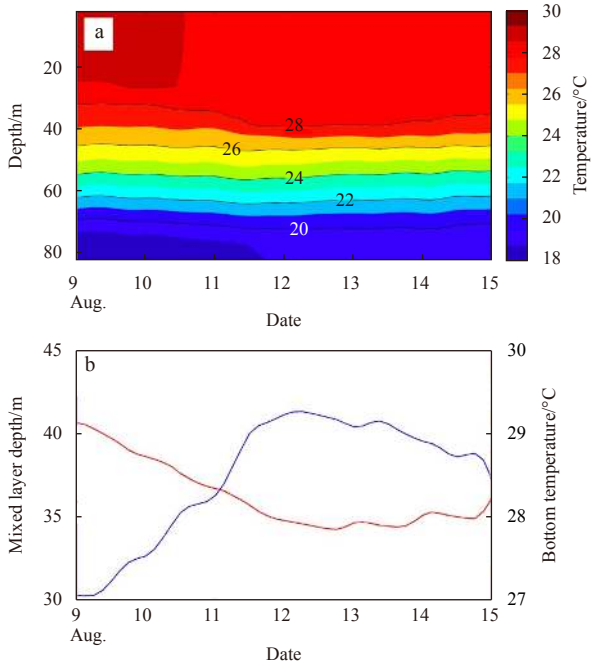

Fig. 7. Temporal evolution of simulated temperature throughout the whole water column (a) and ML depth and temperature at bottom of the ML at the representative grid point A along the typhoon track (b).

The temporal evolution of the ML depth and temperature at bottom of the ML at grid point A is shown in Fig. 7b. On 9 August, Rananim reached the southern ECS. Then, the ML depth increases from about 30 m to a maximum value of over 41 m (deepens by 11 m) on August 12. After the Rananim passage, the ML depth gradually shoals (Fig. 7b). The temperature at bottom of the ML shows that the temperature is about 29.1°C at the beginning. Then, the temperature quickly drops to 27.8°C on August 12 with a maximum cooling of 1.3°C. Once the Rananim disappears, the temperature at bottom of the ML gradually increases.

The temperature change in the ML can be expressed by the following form(Denman and Peña, 2002):

$$\frac{\partial hT}{\partial t} = -wh\frac{\partial T}{\partial z} + h\left(K_z\frac{\partial^2 T}{\partial z^2} + \frac{\partial Q}{\partial z}\right), \tag{1}$$

where t represents the time, T is the temperature in the ML, h is the ML depth. z represents the vertical direction and w is the vertical velocity. K_z is the vertical diffusion coefficient, Q is the surface heat flux.

The term on the left side of Eq. (1) represents the temperature change in the ML. The first term on the right side of Eq. (1) denotes the Ekman-pumped upwelling effect as follows:

$$w = \frac{1}{f\rho_0}\left(\frac{\partial \tau^y}{\partial x} - \frac{\partial \tau^x}{\partial y}\right). \tag{2}$$

Equation (2) means that the wind stress curl can generate vertical velocity with cyclonic wind stress generating upward vertical velocity (upwelling) and anti-cyclonic wind stress generating downward vertical velocity (downwelling). During the Rananim passage, the strong cyclonic wind stress favors an Ekman pumping, which upwells cold water from lower layer and causes a tem-

perature cooling in the ML. The second and third terms on the right side of Eq. (1) together are called the vertical diffusion term (Price, 1981; D'Asaro et al., 2007). Rananim can generate a strong ocean current in the sea surface layer (as shown in the following). The strong vertical current shear causes a well vertical mixing, leading to the temperature decreasing in the whole ML. This process is also called the vertical entrainment. For oceanic response to typhoon, Eq. (1) means that the temperature cooling in the ML is caused by both the Ekman pumping and vertical entrainment.

4.2 *Oceanic current responses*

In this section, we further reveal the oceanic current responses to Rananim. Compared with in the open ocean, the oceanic current responses to a typhoon is much more complicated because of the strong and complex background current in the ECS.

Figures 8 and 9 shows the spatial and temporal evolution of simulated surface current in the ECS during the Rananim passage from 9 to 14 August. In the early stage (Fig. 8a), although Rananim has reached the southern ECS, the background current is not significantly affected. The background current shows well-organized pattern that the KC flows northeastward from east of Taiwan along the ECS slope with a magnitude of over 80 cm/s. On the ECS shelf, the TWC flows northward with a magnitude of 40 cm/s. In the following, the background current is affected: northwestward current is generated on the northern ECS shelf. Then,

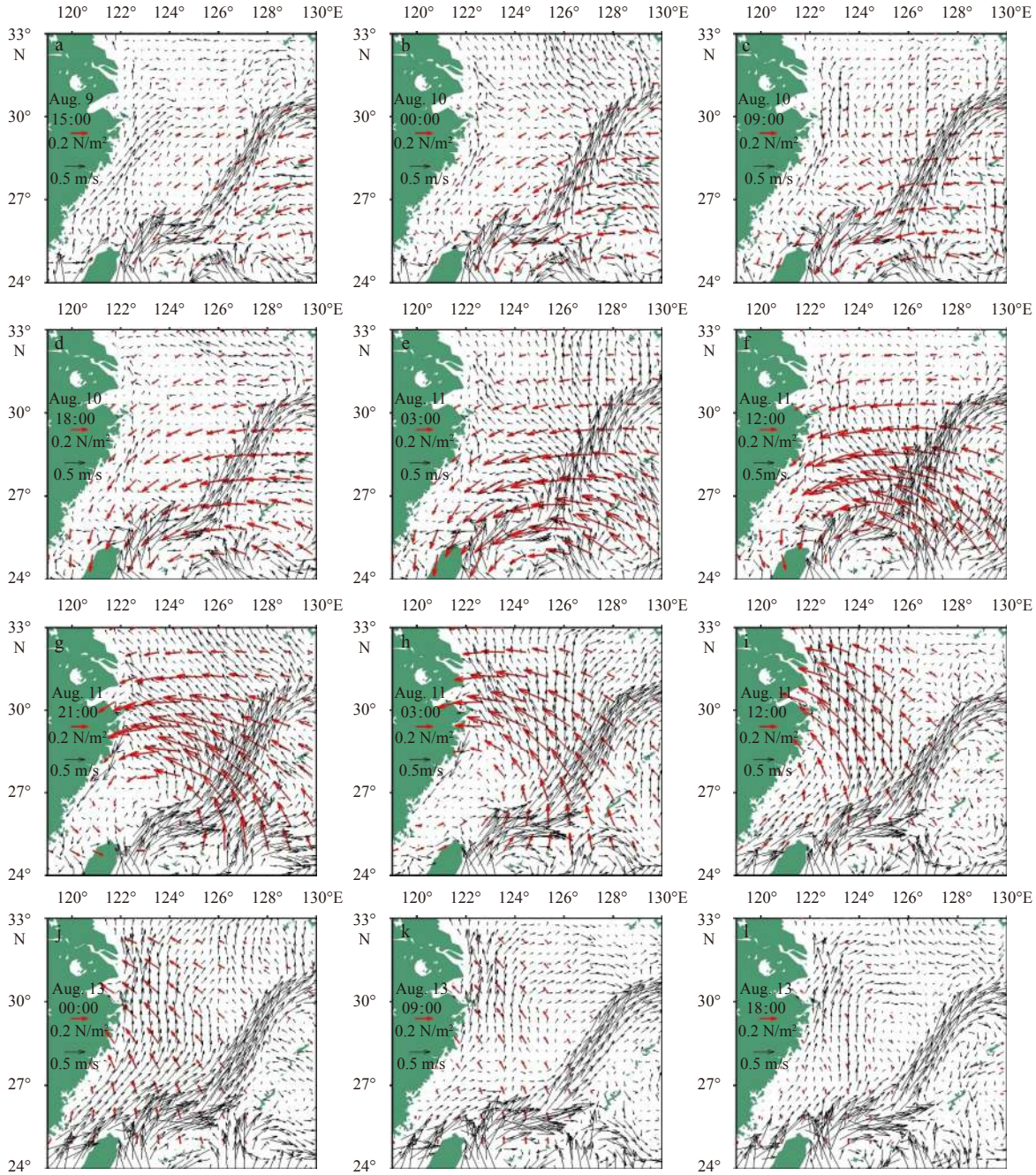

Fig. 8. Spatial and temporal evolution of the simulated surface current during Rananim passes over the ECS. Each snapshot has an interval of 9 h.

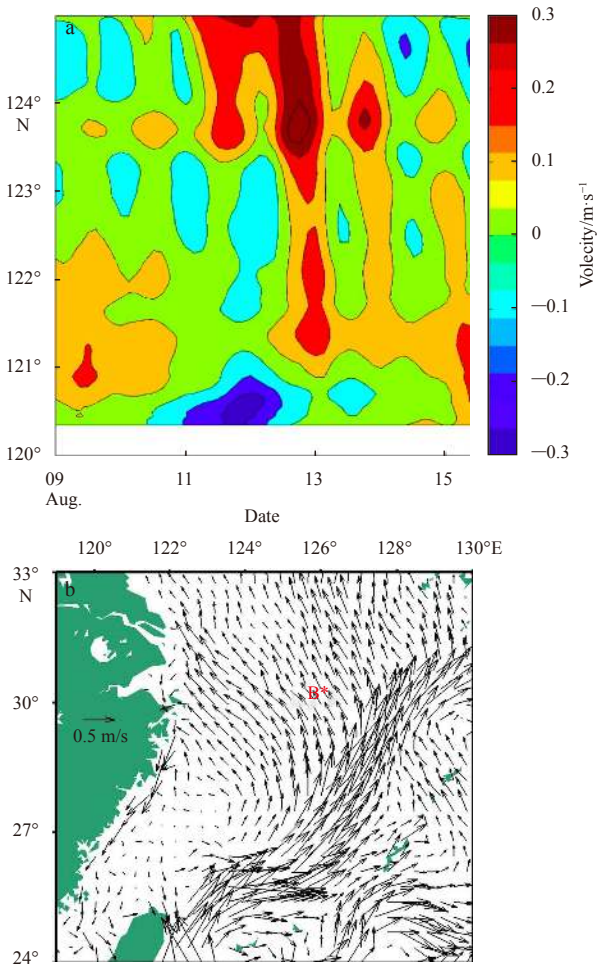

Fig. 9. The temporalvariation of the north component of the surface velocity at the 27°N section of the ECS (a) and simulated surface current at 0 o'clock August 12. The asterisk in Fig. 9b represents a grid point B (27.3°N, 123°E) where the current response is very strong (b).

quickly rotates clockwise (Figs 8b, c). As with the northwestward movement of Rananim, the northward TWC on the southern ECS shelf disappears and strong northwestward current is formed on the whole ECS shelf (Figs 8d–f), especially in the northern ECS. The current in the northern ECS is much stronger, which is because the wind stress is much stronger at the right side of typhoon track (northern ECS). When Rananim lands in the Zhejiang Province of China, the cyclonic wind becomes northward wind (Figs 8h, i). Therefore, the northward wind favors strong northward current on the ECS shelf (Figs 8g–i). At last, Rananim disappears and the strong northward current gradually adjusts to the previous background current on the ECS (Figs 8j, k).

Figure 9 shows the variation in the north component of the surface velocity of the 27°N section of the East China Sea over time. As Typhoon Rananim mainly affects the southern part of the East China Sea, and the flow field is mainly north-south direction, the time evolution of the sea area flow is analyzed more quantitatively through the north component of the surface velocity of the section. It can be seen from the figure that before August 11, in the near-shore area, west of 122.5°E, the northward flow rate is about +10–15 cm/s. This Corresponds to the structure of the Taiwan warm current when the typhoon has not arrived (Figs 8a–d), the position of flow nucleus of the Taiwan warm current is about 121°E. On the east of 122.5°E, the flow velocity of the northward flow apparently began to decrease. From August 11 to August 12, two ends of the section showed an inverse change. At the end near the shore, the flow rate becomes negative, meaning that the northward Taiwan warm current disappears and southward current appears. On the shelf, east of 123.5°E, the forward flow rate is large, indicating that there is a strong northward flow. This cross-sectional distribution corresponds to the flow field variation in Figs 8e–h.

The current response in the whole water column is also very important because it provides an insight into the NIOs information generated by typhoon. Figure 10 shows the temporal evolution of current throughout the whole water column at a representative grid point B (Fig. 9). This location is selected as a representative grid point for two considerations. Firstly, in the northern ECS, the background current is relatively weak. This facilatates to highlight the current generated by Rananim. Secondly, the wind stress is much stronger onthe right side of typhoon track, namely in the northern ECS. This indicates that the current response is much stronger in the northern ECS. Some prominent features are noticeable from Fig. 10. Firstly, during the Rananim passage, the current magnitudes of both u-component and v-component are largely strengthened. Secondly, the water column with large curent magnitudes (u>10 cm/s, v>10 cm/s) deepens from about 20 m to 40 m. Thirdly, the current components show out-of phase variation in the upper and lower layers. Fourthly, strong near inertial currents with upward propagating phase are generared. The first three features are most noticeable on August 12, when the current responses are the most energetic. The strongest northeastward current with a magnitude of over 40 cm/s can even deepen to 40 m layer. In contrast, the fourth feature is not very prominent before August 12. In fact, one can see that strong

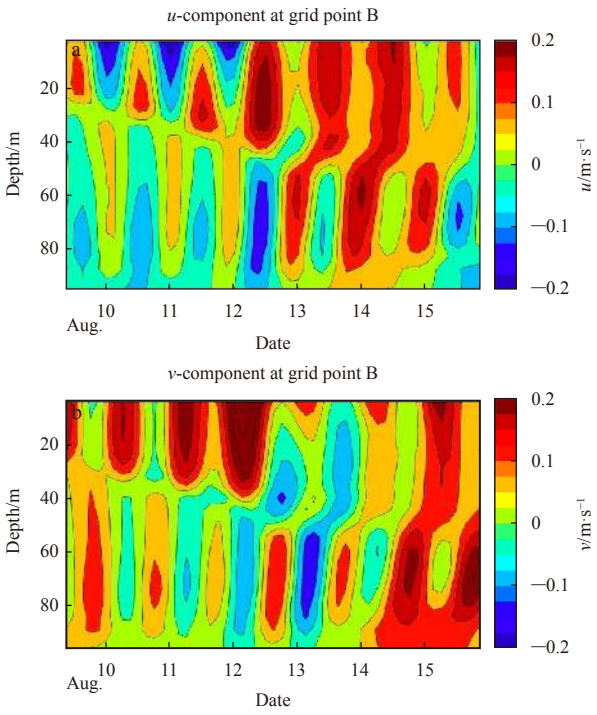

Fig. 10. Temporal evolution of the simulated current for u-component (a) and v-component (b) throughout the whole water column at grid point B.

near inertial currents with upward phase are very prominent from August 13 to 14, when Rananim disappears for one to two days.

Figure 11 shows the power spectra of the surface and bottom current components at grid point B. The most prominent feature of the power spectra is that the four current components all show a large energy peak at 0.95 day period. This precisely reflects the strong near inertial current generated by Rananim. The power spectra (Fig. 11a) shows that the surface u-component (u_s) is more energetic than the bottom u-component (u_b). In contrast, the surface v-component (v_s) is equally energetic as the bottom v-component (v_b) (Fig. 11b).

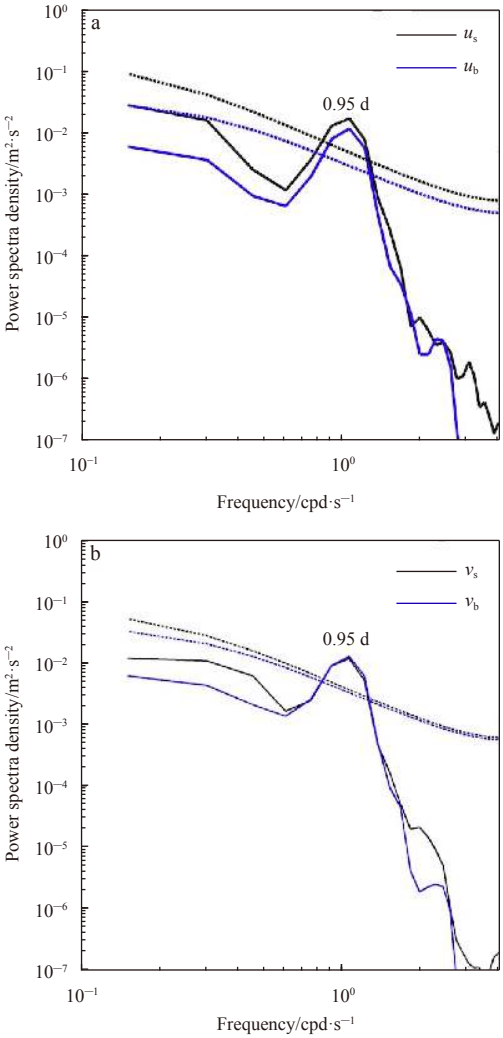

Fig. 11. Power spectra of the surface and bottom of current components at grid point B. The dashed lines indicate the 95% confidence level.

5 Conclusions

In this study, the oceanic responses to Typhoon Rananim on the ECS shelf are investigated from both satellite SST data and numerical simulation. Rananim is a very destructive typhoon in the ECS in August 2004. The satellite observation shows a significant SST cooling of over 3°C on the ECS shelf during the Rananim passage. The numerical model can reasonably simulate the oceanic responses to Rananim although the simulated SST cooling is slightly weaker than the observed one. This is possibly due to the model does not consider the atmosphere-ocean coupling which can improve the simulated results (Li et al., 2002; Wada and Kunii, 2017). The simulated SST cooling shows an evident right-biased feature, which is in good agreement with the observed one. Rananim deepens the ML on the ECS shelf by more than 10 m and causes the whole ML cooling by about 1.3°C. Both Ekman pumping and vertical entrainment are responsible for the thermal response. These features are consistent with the findings of Price (1981), Wentz et al. (2000) and Tsai et al. (2008).

Compared with those current responses to typhoons in the open ocean (Price, 1983; Ko et al., 2014; Zhang et al., 2016), the current responses to Rananim on the ECS shelf are more energetic and complex. Our results show that during the Rananim passage, the background current systems on the ECS shelf are significantly deformed. Rananim can even reverse the strong northward TWC on the ECS shelf. Rananim generates strong surface current which is featured by the Ekman current. Once the surface current is formed, it rotates clockwise quickly (Fig. 8). Price (1983) showed that the NIOs dominate the current responses to typhoon. The strong NIOs are also shown in this study. During the Rananim passage, the strong near inertial currents deepens from 20 m to over 40 m. When Rananim disappears about one day, the strong near inertial currents propagate upward (Fig. 10).

References

Bleck R. 2002. An oceanic general circulation model framed in hybrid isopycnic-Cartesian Coordinates. Ocean Modelling, 4(1): 55–88, doi: 10.1016/S1463-5003(01)00012-9

Brink K H. 1989. Observations of the response of thermocline currents to a hurricane. Journal of Physical Oceanography, 19(7): 1017–1022, doi: 10.1175/1520-0485(1989)019<1017:OOTROT>2.0.CO;2

Brooks D A. 1983. The wake of Hurricane Allen in the western Gulf of Mexico. Journal of Physical Oceanography, 13(1): 117–129, doi: 10.1175/1520-0485(1983)013<0117:TWOHAI>2.0.CO;2

Chiang T L, Wu C R, Oey L Y. 2011. Typhoon Kai-Tak: An ocean's perfect storm. Journal of Physical Oceanography, 41(1): 221–233, doi: 10.1175/2010JPO4518.1

D'Asaro E A, Sanford T B, Niiler P P, et al. 2007. Cold wake of hurricane Frances. Geophysical Research Letters, 34(15): L15609

Denman K L, Peña M A. 2002. The response of two coupled one-dimensional mixed layer/planktonic ecosystem models to climate change in the NE subarctic Pacific Ocean. Deep Sea Research Part II: Topical Studies in Oceanography, 49(24–25): 5739–5757, doi: 10.1016/S0967-0645(02)00212-6

Emanuel K A. 1999. Thermodynamic control of hurricane intensity. Nature, 401(6754): 665–669, doi: 10.1038/44326

Gentemann C L, Meissner T, Wentz F J. 2010. Accuracy of satellite sea surface temperatures at 7 and 11 GHz. IEEE Transactions on Geoscience and Remote Sensing, 48(3): 1009–1018, doi: 10.1109/TGRS.2009.2030322

Jacob S D, Shay L K, Mariano A J, et al. 2000. The 3D oceanic mixed layer response to Hurricane Gilbert. Journal of Physical Oceanography, 30(6): 1407–1429, doi: 10.1175/1520-0485(2000)030<1407:TOMLRT>2.0.CO;2

Kalnay E, Kanamitsu M, Kistler R, et al. 1996. The NCEP/NCAR 40-year reanalysis project. Bulletin of the American Meteorological Society, 77(3): 437–472, doi: 10.1175/1520-0477(1996)077<0437:TNYRP>2.0.CO;2

Ko D S, Chao S Y, Wu C C, et al. 2014. Impacts of Typhoon Megi (2010) on the South China Sea. Journal of Geophysical Research: Oceans, 119(7): 4474–4489, doi: 10.1002/2013JC009785

Li Zhiyuan, Huang Daji, Xing Chuanxi, et al. 2019. The synoptic variation of Yellow Sea Warm Current in winter and its mechanisms. International Journal of Numerical Methods for Heat & Fluid Flow, 29(2): 724–737

Li Zhiyuan, Huang Daji. 2019. Sea surface height and current responses to synoptic winter wind in the Bohai, Yellow, and East

China Seas: Two leading coastal trapped waves. Journal of Geophysical Research: Oceans, 124(4): 2289–2312, doi: 10.1029/2018JC014120

Li Yongping, Xue Huijie, Bane J M. 2002. Air-sea interactions during the passage of a winter storm over the Gulf Stream: A three-dimensional coupled atmosphere-ocean model study. Journal of Geophysical Research: Oceans, 107(C11): 3200, doi: 10.1029/2001JC001161

Marshall J, Adcroft A, Hill C, et al. 1997. A finite-volume, incompressible Navier Stokes model for studies of the ocean on parallel computers. Journal of Geophysical Research: Oceans, 102(C3): 5753–5766, doi: 10.1029/96JC02775

Price J F. 1981. Upper ocean response to a hurricane. Journal of Physical Oceanography, 11(2): 153–175, doi: 10.1175/1520-0485(1981)011<0153:UORTAH>2.0.CO;2

Price J F. 1983. Internal wave wake of a moving storm. Part I. Scales, energy budget and observations. Journal of Physical Oceanography, 13(6): 949–965, doi: 10.1175/1520-0485(1983)013<0949:IWWOAM>2.0.CO;2

Shay L K, Elsberry R L. 1987. Near-inertial ocean current response to Hurricane Frederic. Journal of Physical Oceanography, 17(8): 1249–1269, doi: 10.1175/1520-0485(1987)017<1249:NIOCRT>2.0.CO;2

Shay L K. 2010. Air-sea interactions in tropical cyclones. Global Perspectives on Tropical Cyclones, 4: 93–131

Tsai Y, Chern C S, Wang J. 2008. Typhoon induced upper ocean cooling off northeastern Taiwan. Geophysical Research Letters, 35(14): L14605, doi: 10.1029/2008GL034368

Wada A, Kunii M. 2017. The role of ocean-atmosphere interaction in Typhoon Sinlaku (2008) using a regional coupled data assimilation system. Journal of Geophysical Research: Oceans, 122(5): 3675–3695, doi: 10.1002/2017JC012750

Wentz F J, Gentemann C, Smith D, et al. 2000. Satellite measurements of sea surface temperature through clouds. Science, 288(5467): 847–850

Wright R. 1969. Temperature structure across the Kuroshio before and after typhoon Shirley. Tellus, 21(3): 409–413, doi: 10.3402/tellusa.v21i3.10096

Yang Bing, Hou Yijun, Hu Po, et al. 2015. Shallow ocean response to tropical cyclones observed on the continental shelf of the northwestern South China Sea. Journal of Geophysical Research: Oceans, 120(5): 3817–3836, doi: 10.1002/2015JC010783

Zhang Han, Chen Dake, Zhou Lei, et al. 2016. Upper ocean response to typhoon Kalmaegi (2014). Journal of Geophysical Research: Oceans, 121(8): 6520–6535, doi: 10.1002/2016JC012064